Research Article

For reprint orders, please contact reprints@future-science.com

Future Medicinal Chemistry

N-heterocyclic carbene complexes of silver and gold as novel tools against breast cancer progression

Aim: Metal carbenic complexes have received considerable attention in both the catalysis and biological fields for their potential applications in cancer and antimicrobial therapies. **Results:** A small series of new silver and gold N-heterocyclic carbene complexes has been designed and synthesized. Among the tested complexes, one compound was particularly active in inhibiting anchorage-dependent and -independent breast cancer proliferation, and inducing cell apoptosis via a mitochondria-related process. The antitumor activity was associated to the transcriptional activation of the tumor suppressor gene *p53* in an Sp1-dependent manner, as evidenced by biological and docking studies. **Conclusion:** Our results highlight the importance and the versatility of *N*-heterocyclic carbene complexes of gold and silver as useful tools against breast cancer progression.

First draft submitted: 31 May 2016; Accepted for publication: 19 September 2016; Published online: 22 November 2016

Keywords: breast cancer • mitochondria • N-heterocyclic carbene complexes • p53 • Sp1 • transmetallation

Carmela Saturnino**[‡,1], Ines Barone[‡,2], Domenico Iacopetta[2], Annaluisa Mariconda[3], Maria Stefania Sinicropi*, Camillo Rosano*[,4], Antonella Campana[2], Stefania Catalano[2], Pasquale Longo[†,3] & Sebastiano Andò[†,2]

[1]Department of Pharmacy, University of Salerno, 84084 Fisciano, Salerno, Italy

[2]Department of Pharmacy, Health & Nutritional Sciences, University of Calabria, 87036 Arcavacata di Rende, Italy

[3]Department of Chemistry & Biology, University of Salerno, 84084 Fisciano, Salerno, Italy

[4]UOS Proteomics IRCCS AOU San Martino-IST National Institute for Cancer Research, Largo R. Benzi 10, Genoa, Italy

*Author for correspondence:
Tel.: +39 0984 493200
Fax: +39 0984 493107
s.sinicropi@unical.it

**Author for correspondence:
Tel.: +39 010 5558337
Fax: +39 010 555 8228
camillo.rosano@hsanmartino.it

[†]Joint senior authors

[‡]Authors contributed equally

Breast cancer represents the most frequently diagnosed cancer and the leading cause of cancer death in women worldwide, with approximately 1.7 million cases (25% of all cancers) and 521,900 deaths recorded in 2012 [1]. Based on both tumor biology and clinical factors, breast cancers are usually treated with a combination of surgery, radiotherapy, endocrine therapy (e.g., tamoxifen), biologic therapy (e.g., herceptin) and chemotherapy (e.g., platinum-based agents). Chemotherapy regimens are also currently used as treatment of choice for advanced-stage/metastatic disease, but are associated with severe adverse effects. Indeed, the most widely used platinum-based anticancer drug *cis*-platin has several limitations, such as neurotoxicity, nephrotoxicity, ototoxicity and development of intrinsic and acquired resistance in some cancer cells [2]. In addition, *cis*-platin presents a limited aqueous solubility, and is chemically incompatible with thiols. Therefore, looking for novel antitumoral metal-containing molecules with lower toxicity and higher stability is urgently needed to prolong patient survival and improve their quality of life.

Recently, several metal complexes have been investigated for their potential anticancer activities [3–9]. Among them, metal *N*-heterocyclic carbene (NHC) complexes are receiving growing interest in pharmaceutical research, as they readily fit the requirements for an efficient drug design, fast optimization and stability [10–12]. These complexes have the general formula L_nMX_m (Figure 1), where M is the metal that constitutes the center of the reaction, L is the carbene, namely the ligand capable of influencing the electronic properties of the metal and, consequently, the possible catalytic activity of the complex and X is a not carbenic ligand. In most cases, it can be a halide, a carboxylate or an alkoxide anion. A particular type of carbene is L_nM in which the metal has an oxidation state equal to 0.

FUTURE SCIENCE part of fsg

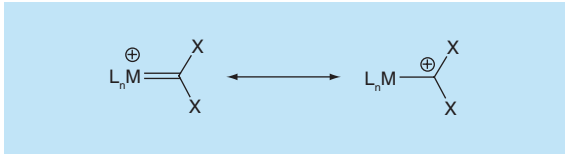

Figure 1. Carbene metal complex structures.

Three types of complexes between a carbene and a transition metal have been described so far by Fischer [13], Schrock [14,15] and Arduengo-Wanzlick [16]. Chemically, they are able to form strong coordinate covalent bonds with various transition metal centers through σ-donation and p-back-donation, and saturation or aromaticity of the NHC ligand and the volume of attached side chains influence the stability and reactivity of the complexes [17–19]. Taking advantage of their fascinating chemical properties, different examples of NHC complexes of silver and gold have been biologically evaluated, but also platinum or other transition metals seem to have promising properties in biomedical sciences [7,20–23]. In particular, Ag–NHCs have long been used as antimicrobial agents for their high stability [24], as they can overcome the drawbacks associated with conventional silver antibiotics including resistance and fast loss of activity [25–27]. Some of them also exhibited *in vitro* antitumor effects [28]. However, the Ag complexes may display less cytotoxic activity than the corresponding Au complexes toward cancer cell lines [29]. Indeed, Au–NHCs exhibit a wide range of biological activities, including antiarthritic [30] antimicrobial [31] and especially antitumor ones. Over the last 10 years, there were a growing number of literature reports regarding the anticancer properties of Au (I/III)–NHC complexes in different cellular background, such as melanoma, breast, prostate and hepatocellular carcinoma cell lines. It has been proved that Au–NHC complexes can differently impact cell cycle distribution, expressions of several key regulators of apoptosis, caspase activation, mitochondrial integrity and intracellular reactive oxygen species (ROS) generation [32–35]. For instance, a recent paper has shown that an Au–NHC complex was able to induce antimelanoma effects *in vitro* and *in vivo* by p53 upregulation [36].

Due to this knowledge, the main goal of the present report was to synthesize novel NHC complexes of silver and gold, whose structures were realized to evaluate the influence of increased lipophilicity on their pharmacological effects, as known from the literature [37]. Indeed, the lipophilic cation delocalized can pass through biological membranes more quickly and concentrate into organelles, mainly in the mitochondria, of cancer cells. NHC-ligand lipophilicity was increased through the functionalization of the nitrogen atoms with lipophilic substituents. Starting from the imidazole, it was evaluated the effect of different substituents on N-1 atom on the pharmacological activity. Particularly, the position 1 was substituted with a 2-cyclopentanol (L1), 2-cycloesanol (L2) and 2-hydroxy-2-phenylethyl (L3) side chains and in position 3 a methyl group was always present (Figure 2). Moreover, we prepared silver and gold NCH-complexes with the aim to evaluate the importance of the metal (i.e., silver in **AgL1**, **AgL2**, **AgL3** and gold in **AuL1**, **AuL2** and **AuL3**). The obtained complexes have been studied for their antitumor properties in human breast cancer cells and the underlying molecular mechanism has been investigated in detail by biological assays and macromolecular docking studies, in order to shed more light on the possible ligand–protein binding modes. Specifically, we have demonstrated that one of the tested compound, **AuL3**, was particularly active in inhibiting growth and inducing apoptosis of breast cancer cells, without exerting any effects in normal breast epithelial cells. Mechanistically, this compound was able to bind the transcription factor Sp1 and to stimulate the transcription of the tumor suppressor gene *p53* in an Sp1-dependent manner.

Materials & methods

Chemistry

All manipulations were carried out under oxygen- and moisture-free atmosphere in an MBraun MB 200 glove-box. All the solvents were thoroughly deoxygenated and dehydrated under argon by refluxing over suitable drying agents; while NMR deuterated solvents (Euriso-Top products) were kept in the dark over molecular sieves.

The organic compounds imidazole, styrene oxide, cyclohexene oxide, cyclopentene oxide and iodomethane (Strem Chemicals Inc., Kehl, Germany; Sigma-Aldrich Chemie GmbH, Steinheim, Germany) were used as received. The silver (I) oxide Ag_2O was purchased from Sigma-Aldrich (Sigma-Aldrich Chemie GmbH, Steinheim, Germany). ^{1}H NMR, homodecoupled ^{1}H NMR and ^{13}C NMR spectra were recorded at 298 K on a Bruker Avance 400 spectrometer operating at 400 MHz (^{1}H) and 100 MHz (^{13}C) and referred to internal tetramethylsilane. Fourier transform infrared (FTIR) spectra were obtained at a resolution of 2.0 cm^{-1} with a Bruker-Vector 22 FTIR spectrometer equipped with a deuterated triglycine sulfate detector and Ge/KBr beam splitter. The frequency scale was internally calibrated to 0.01 cm^{-1} using an He–Ne reference laser. Thirty-two scans were signal-averaged to reduce spectral noise. ESI-MS spectra were performed on a Quattro Micro triple quadrupole mass spectrometer equipped with an electrospray ion source. The elemental analyses for C, H, N were recorded on a Thermo-Finnigan Flash EA 1112 and were performed

according to standard microanalytical procedures. The elemental analyses for I, Ag were carried out by atomic absorption spectrophotometer AAnalyst model 100 (PerkinElmer, MA, USA) equipped hollow-cathode lamp Lumina Au (PerkinElmer) using the software AAwinLabAnalyst. Gold was determined with a burner (FIAS-100) air-acetylene flame. Solution of Au at known concentration prepared from a stock solution of 1 g/l (Carlo Erba, Milan, Italy) was used as standards. The instrument was set at zero using a 1% solution of HNO_3. Sample scripts were analyzed along with their white. Chloride was determined indirectly by reaction of $AgNO_3$ with Cl^-, precipitation of AgCl which was dissolved in $Na_2S_2O_3$. Silver content in the solution was determined by Flame Atomic Absorbtion Spectroscopy (FAAS) and the chloride content was calculated using the content of silver. The molar conductance of 10^{-3} M solutions of the gold complexes in CH_2Cl_2 solvent were measured on a Mettler Toledo Conductivity Sensor LE703 model. All the measurements were taken at room temperature for freshly prepared solutions.

Synthesis of proligands & of silver(I)-NHC complexes

The synthesis of imidazolium salts (imidazolium *N*-methyl-*N*′-cyclopentan-2-ol-iodide **L1**, imidazolium-*N*-methyl-*N*′-cyclohexane-2-ol-iodide **L2,** *N*-methyl-*N*′-[(2-hydoxy-2-phenyl)ethyl] imidazolium iodide **L3**) and of the respective silver complexes (**AgL1, AgL2, AgL3**) were carried out in the same way as reported in [38].

Synthesis of gold(I)-NHC complexes

Complexes **AuL1, AuL2** and **AuL3** were synthesized by transmetallation between the appropriate Ag(I)–NHC complex (**AgL1, AgL2, AgL3**) and chloro(dimethylsulfide)gold(I) [(Me_2S)AuCl] according to the reported procedure in the literature [39].

General procedure

To a solution of the silver complex (**AgL1** or **AgL2** or **AgL3**) in CH_2Cl_2 a stoichiometric amount of (Me_2S)AuCl was added. The mixture was left to stir for 4 h at room temperature. After this time it was filtered through celite and the solvent was removed *in vacuo*. The crude product was washed in hexane to obtain a yellow powder in good yield.

Complex AuL1 (bis-[N-methyl, N´(cyclopentane-2ol)-imidazole-2-ylidine]gold(I)]+[di-chloro-gold]-)

For the synthesis of **AuL1** the amount of silver complex precursor *AgL1* was $7{,}21 \bullet 10^{-4}$ mol in 51,5 ml of CH_2Cl_2.

Yield: 46,7%.

^{1}H NMR (400 MHz, CD_2Cl_2): 6.94 (s,1H, NC*H*CH), 7.01 (s, 1H, NCHC*H*), 4.81 (m, 1H, OC*H*), 4.47 (m, 1H, NC*H*), 3.83 (s, 3H, NCH_3), 2.56 (m, 2H, $OCHCH_2$), 2.24 (m, 2H, $NCHCH_2$), 1.75 (m, 2H, $CH_2CH_2CH_2$).

^{13}C NMR (100 MHz, CD_2Cl_2): 169.5 (N*C*N), 124.5 (N*C*HCH,) 122.0 (NCH*C*H), 78.4 (O*C*H), 69.5 (N*C*H), 45.6 (NCH_3), 39.9 ($OCHCH_2$), 34.0 ($NCHCH_2$), 28.2 ($CH_2CH_2CH_2$).

Elemental analysis: found (%):C 27.12; H 3.64; Au 49.45; Cl 8.62; N 6.96; O 3.89 Calc. for $C_9H_{15}AuClN_2O$ (%): C 27.05; H 3.78; Au 49.29; Cl 8.87; N 7.01; O 4.00.

Mass spectrum: 531 $[Au(L1)_2]^+$.

Complex AuL2 (bis-[N-methyl, N´(cyclohexane-2ol)-imidazole-2-ylidine] gold(I)]+[di-chloro-gold]-)

For the synthesis of **AuL2** the amount of silver complex precursor *AgL2* was $1{,}25 \cdot 10^{-3}$ mol in 89 ml of CH_2Cl_2.

Yield: 49,9%.

^{1}H NMR (400 MHz, CD_2Cl_2): 6.99 (s,1H, NC*H*CH), 7.01 (s, 1H, NCHC*H*), 5,48 (s, 1H, O*H*CH) 4.48 (m, 1H, OC*H*), 3.62 (m, 1H, NC*H*), 3.69 (s, 3H, NCH_3), 2.29 (m, 2H, $OCHCH_2$), 2.00 (m, 2H, $NCHCH_2$), 1.57 (m, 2H, $OCHCH_2CH_2$), 1.40 (m, 2H, $NCHCH_2CH_2$).

^{13}C NMR (100 MHz, $CDCl_3$): 178.9 (N*C*N), 131.5 (N*C*HCH,) 126.9 (NCH*C*H), 72.9 (O*C*H), 67.4 (N*C*H), 43.8 (NCH_3), 41.9 ($OCHCH_2$), 35.1 ($NCHCH_2CH_2$), 33.2 ($NCHCH_2$), 26.8 ($OCHCH_2CH_2$).

Elemental analysis: found (%):C 29.3; H 4.02; Au 47.81; Cl 8.49; N 6.91; O 3.72. Calc. for $C_{10}H_{17}AuClN_2O$ (%): C 29.03; H 4.14; Au 47.61; Cl 8.57; N 6.77; O 3.87.

Mass spectrum: 559 $[Au(L2)_2]^+$.

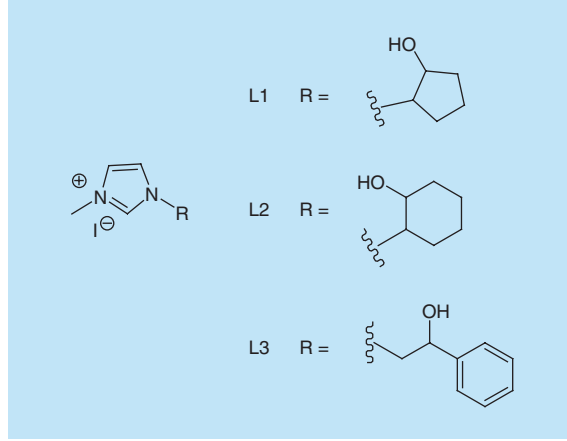

Figure 2. NHC proligands L1, L2 and L3.

Complex AuL3 bis-[N-methyl, N´(2-hydroxy-2-phenyl)ethyl)-imidazole-2-ylidine]gold(I)]+[dichloro-gold]-)

For the synthesis of **AuL3** the amount of silver complex precursor *AgL3* was 5,32•10^{-4} mol in 38 ml of CH_2Cl_2.

Yield: 71,8%.

^{1}H NMR (400 MHz, CD_2Cl_2): δ 7.31–7.41 (m, 5H, *Ph ring*); 7.05 (d, 1H, NC*H*CHN); 6.99 (d, 1H, NCHC*H*N); 4.31 (t, 1H, C*H*OH); 3.94 (d, 2H, NCH_2); 3.71 (s, 3H, NCH_3).

^{13}C NMR (100 MHz, CD_2Cl_2): δ 185.0 (N*C*N); 141.8, 129.2, 127.5, 126.6 (*Ph ring*); 122.9 (N*C*HCHN), 122.0 (NCH*C*HN), 75.2 (O*C*H_2), 59.3 (N*C*H_2), 41.0 (N*C*H_3).

Elemental analysis: found (%):C 33.29; H 3.34; Au 45.42; Cl 8.01; N 6.54; O 3.53. Calc. for $C_{12}H_{15}AuClN_2O$ (%): C 33.08; H 3.47; Au 45.21; Cl 8.14; N 6.43; O 3.67.

Mass spectrum: 603 $[Au(L3)_2]^+$.

Docking studies

The initial structures of **AuL3** and **AgL3** were designed and optimized in PRODRG server [40]. Docking simulations were performed using the program GOLD v.5.2.2 [41]; residues Phe 3, Ser 15, Leu 18, Ser 19, Ile 22, Lys 23 and Gln 26 were defined with flexible side chains (i.e., a free rotation of their side chains was allowed). Simulations were performed using the standard defaults: for both the molecules the number of islands was set to 5, population size to 100, number of operations 100,000, the niche size of 2 and a selective pressure 1.1. ChemPLP scoring was used. Figures were drawn with the program Chimera [42,43].

Biological procedures

Plasmids

The different *p53* luciferase reporter constructs, named as *p53*-1, -6, and -13, were provided by S Safe (Texas A&M University, TX, USA) and were generated from the human *p53* gene promoter as it follows: *p53*-1 (comprising the -1800 to +12 region), *p53*-6 (comprising the -106 to +12 region), *p53*-13 (comprising the -106 to -40 region) [44].

Cell culture

Human nontumorigenic MCF-10A breast epithelial cells were cultured in Dulbecco's modified Eagle's medium-F12 supplemented with 5% Horse Serum, 0.5 µg/ml hydrocortisone, 20 ng/ml human EGF, 100 ng/ml Cholera toxin and 10 µg/ml insulin. Human ER-positive MCF-7 and ZR-75-1 breast cancer cells were cultured in DMEM-F12 medium containing 5% Newborn Calf Serum, or 5% Fetal Bovine Serum, respectively. All media were supplemented with 2 mmol/l L-glutamine and 1 mg/ml penicillin–streptomycin. Subconfluent cell cultures, synchronized for 48 h in DMEM-F12 without phenol red and serum (SFM), were used for all reported experiments.

Cell proliferation assays

MTT anchorage-dependent growth assays

Cell viability was determined by using the 3-(4,5-dimethylthiazol-2-y1)-2,5-diphenyltetrazolium (MTT, Sigma-Aldrich, Milan, Italy) assay, as previously described [45–47]. Briefly, cells (2 × 10^4 cells/well) were plated in 24-well plates and treated as indicated. After 72 h, 100 µl of MTT stock solution in PBS (2 mg/m1) was added into each well and incubated for 2 h at 37°C followed by removal of media and solubilization in 500 µl of dimethyl sulphoxide. Plates were shaken for 15 min, and the absorbance was measured at 570 nm in each well, including the blanks. At least three experiments, each one performed with seven different doses of **AuL3, AgL3** and *cis*-platin in triplicate were combined for IC_{50} calculations. The IC_{50} was determined using GraphPad Prism 4 Software (GraphPad Inc., CA, USA), as previously reported [48].

Soft agar anchorage-independent growth assays

Soft agar growth assays were performed as indicated in [49]. Briefly, cells (10^4/well) were plated in 4 ml of 0.35% agarose with 5% charcoal stripped-FBS in phenol red-free media, with a 0.7% agarose base in six-well plates. Forty-eight hours after plating, medium containing vehicle or the different treatments was added to the top layer, and replaced every 48 h. After 15 days, 200 µl of MTT was added to each well and incubated for 4 h at 37°C. Plates were then placed overnight at 4°C and colonies >50 µm diameter were counted. The data are representative of three independent experiments, each performed in triplicate.

TUNEL assay

Cell apoptosis was investigated by TUNEL assay, following the manufacturer's instructions (CF™488A TUNEL Assay Apoptosis Detection Kit, Biotium, Fremont, CA, USA) with small modifications. Briefly, MCF-7 cells were grown on glass coverslips, starved and then treated with **AuL3** 1 µM for 24 h, washed three times with PBS, then methanol-fixed at -20°C for 15 min. Fixed cells were washed three-times with 0.01% (V/V) Triton X-100 in PBS and incubated with 100 µl of TUNEL Equilibration Buffer for 5 min. After removal of Equilibration Buffer, 50 µl of TUNEL reaction mix containing 1 µl of terminal deoxynucleotidyl transferase were added and incubated for 3 h at 37°C in a humid dark chamber. After the incubation, samples were washed three-times with PBS containing 0.1%

Triton X-100 and 5 mg/ml bovine serum albumin and stained with 2-(4-amidinophenyl)-6-indolecarbamidine dihydrochloride (DAPI, Sigma-Aldrich) (0.2 µg/ml) for 10 min in a humidified dark chamber at 37°C. After three additional washes with cold PBS, a drop of mounting solution was added. Cells were observed and imaged under an inverted fluorescence microscope (20× magnification) with excitation/emission wavelength maxima of 490 nm/515 nm (CF™488A) or 350 nm/460 nm (DAPI). Images are representative of three separate experiments.

Mitochondrial staining

For detection of mitochondria, cells were labeled at 37°C for 20 min with the MitoTracker Deep Red fluorescent probe (0.01 mM, Invitrogen, Carlsbad, CA, USA). After the incubation, the probe was washed out with Hank's balanced salt solution, and cell were fixed with 4% paraformaldehyde. Samples were observed and photographed with OLYMPUS-BX51 microscope equipped with a 100× oil immersion objective. Intensity of fluorescence was analyzed with Scion Image Analyzer program (Scion Corporation) and associated p-values were determined for the biological replicates by using GraphPad Prism4 Software. Images are representative of three independent experiments.

Immunoblotting analysis

Protein lysates were subjected to SDS-PAGE, as previously described [50]. After harvesting cells in cold PBS and resuspending them in lysis buffer 20 mmol/l HEPES (pH 8), 0.1 mmol/l EGTA, 5 mmol/l MgCl2, 0.5 M NaC1, 20% glycerol, 1% Triton and protease inhibitors (0.1 mmol/l sodium orthovanadate, 1% phenylmethylsulfonylfluoride and 20 mg/ml aprotinin) for total protein extracts; 250 mmol/l sucrose, 10 mmol/l HEPES (pH = 8), 10 mmol/l KCl, 1,5 mmol/l $MgCl_2$, 1 mmol/l EDTA (pH = 8), 1 mmol/l EGTA (pH = 8), 0,1% digitonin, 1 mmol/l phenylmethylsulfonylfluoride for cytosolic protein extracts, equal amounts of lysates were resolved on a 11–14% SDS-polyacrylamide gel, transferred to a nitrocellulose membrane and probed with antibodies directed against p53, $p21^{WAF1/Cip1}$, PARP, cytochrome c, Bcl2, Bax, BID and GAPDH (Santa Cruz Biotechnology, TX, USA). The antigen–antibody complex was detected by incubation of the membranes for 1 h at room temperature with peroxidase-coupled goat antimouse or antirabbit IgG and revealed using the enhanced chemiluminescence system (Amersham Pharmacia, Milan, Italy). The intensity of bands representing relevant proteins was measured by Scion Image laser densitometry scanning program (Scion Corporation), and standard deviations and associated p-values were determined for the biological replicates by using GraphPad Prism4 Software. Immunoblots show one representative image of three separate experiments.

Real-time RT-PCR assays

Cells were grown in 10 cm dishes to 70–80% confluence and exposed to vehicle or the different treatments as indicated. Total cellular RNA was extracted using TRIZOL reagent (Invitrogen), as suggested by the manufacturer. The purity and integrity were checked spectroscopically and by gel electrophoresis before carrying out the analytical procedures. Analysis of *p53* and $p21^{WAF1/Cip1}$ gene expression was performed by real-time reverse transcription-PCR in the iCycler iQ Detection System (BioRad, Milan, Italy), using SYBR Green Universal PCR Master Mix (BioRad), following the manufacturer's recommendations. Each sample was normalized on the base of its *GAPDH* content. Primers used for the amplification were as following: forward 5′- TCAGTCTACCTCCCGCCATA-3′ and reverse 5′-TTACATCTCCCAAACATCCCT-3′ (*p53*); forward 5′- GCATGACAGATTTCTACCACTCC -3′ and reverse 5′- AAGATGTAGAGCGGGCCTTT -3′ (*p21*); forward 5′-CCCACTCCTCCACCTTTGAC-3′ and reverse 5′-TGTTGCTGTAGCCAAATTCGTT-3′ (*GAPDH*, house-keeping gene).

Luciferase reporter gene assay

MCF-7 cells (5×10^4 cells/well) were plated into 24-well plates with 500 µl of regular growth medium. After 24 h, the medium was replaced with SFM, and transfection was performed by using the FuGENE 6 (Roche Diagnostic, Monza, Italy) reagent as recommended by manufacturer's protocol with the mixture containing 0.5 µg/well p53-1, p53-6 or p53-13 reporter plasmids. After 24 h, the medium was removed and cells were treated with **AuL3** compound as indicated for 24 h. TK Renilla luciferase plasmid (25 ng/well) was used to normalize the efficiency of the transfection. Firefly and Renilla luciferase activities of triplicate samples were measured using a Dual Luciferase kit (Promega, Milan, Italy).

Chromatin immunoprecipitation assays

MCF-7 cells were treated with **AuL3** compound for 3 h, crosslinked with formaldehyde (1%) and then sonicated. Salmon sperm DNA/protein A-agarose was used to immunoclear supernantants (1 h, 48°C). The precleared chromatin was immunoprecipitated with specific anti-Sp1, or antipolymerase II antibodies (Santa Cruz Biotechnology). As a negative control, a normal mouse serum IgG was used. Pellets were

washed, eluted with an elution buffer containing 1% SDS and 0.1M $NaHCO_3$ and digested with the proteinase K. DNA was obtained by phenol/chloroform/isoamyl alcohol extractions and then precipitated with ethanol. Each sample and input (5 µl) were used for real-time PCR. Real-time PCR was performed in the iCycler iQ Detection System (BioRad), using SYBR Green Universal PCR Master Mix (BioRad) with the dissociation protocol used for gene amplification. The primers flanking the Spl sequence present in the *p53* promoter region were the following: 5′- TTCCCCTCCCATGTGCTCAAG-3′ and 5′ -CCAATCCAGGGAACGTGTCA-3′. Final results were calculated using the DDC_t method, using input Ct values instead of the *GAPDH*. As calibrator, the basal sample (vehicle-treated cells) was used.

Statistical analysis

Data were analyzed for their statistical significance using a two-tailed student's t-test ($p < 0.05$, Graph Pad Prism 4). SDs are shown.

Results & discussion

Chemistry & synthesis

Imidazolium-*N*-methyl-*N*′-cyclopentan-2-ol-iodide (**L1**), imidazolium-*N*-methyl-*N*′-cyclohexane-2-ol-iodide (**L2**), *N*-methyl, *N*′-[(2-hydoxy-2-phenyl) ethyl]-imidazolium iodide (**L3**) were prepared by reaction of imidazole with cyclopenteneoxide, cyclohexeneoxide and 1,2-epoxyethylbenzene, respectively, to obtain the monoalkylated product after the opening of epoxy-ring. The second reaction step, by which the second nitrogen atom is methylated using CH_3I, produces the racemic mixture of the salts. In Figure 3 is reported, as an example, the reactions to obtain the pro-ligand L-3. This synthetic strategy was proposed by Arnold *et al.*, and the procedures were previously reported by some of us [51,52].

Silver complexes bearing [NHC] ligands

The salts were reacted with silver oxide (Ag_2O) in inert nitrogen atmosphere. In these conditions, as earlier reported, the silver oxide deprotonates the carbon 2 giving the corresponding Ag–NHC complex [38,53]. Mass spectrometry was of primary importance in determining the structure the structure of Ag–NHC compounds [54,55]. The complexes consist of $[(NHC)_2Ag]^+$ cation and of $[AgI_2]^-$ anion (see Figure 4) as has been conclusively shown by the solid-state structure determined by x-ray diffraction [53].

Gold complexes bearing [NHC] ligands

Complexes **AuL1**, **AuL2** and **AuL3** were synthesized by transmetallation in dichloromethane (CH_2Cl_2), between the corresponding Ag–NHC complex and the gold(I)-cloro-(dimethylsulfide) [$(Me_2S)AuCl$] according to the procedure reported by Baker *et al.* [39]. In Equation (1) is reported **AuL1** as example.

$$AgL1 + (Me_2S)AuCl \xrightarrow{CH_2Cl_2} AuL1 \quad (1)$$

A stoichiometric amount of $(Me_2S)AuCl$ was added to a solution of the silver complex **AgL1** in CH_2Cl_2. Following the procedure reported in the experimental part, a yellow powder in good yield (46,7%) was obtained, whose MS spectrum showed a maximal peak at 531 m/z. FTIR analysis revealed -OH absorbance at 3400 cm^{-1}, and ^1H and ^{13}C NMR spectra gave the expected signals (see the 'Experimental' section), with one sharp carbene resonance at 169.5 ppm. Elemental analysis of **AuL1** found for $C_9H_{15}AuClN_2O$ is in agreement with that calculated (see the 'Experimental' section). Mass spectrometry can provide fundamental data on the structure of compounds in the gas phase. In fact, the maximal peak intensity at 531 m/z is attributable to $[(L1)_2Au]^+$, on the other hand the elemental analysis gives a molar ratio among gold, ligand and chloride of 1:1:1. These data suggest that, as in the case of silver compounds, [38] the gold complex may consist of $[(L1)_2Au]^+$cation and of $[AuCl_2]^-$ anion. The proposed structure was supported by conductivity measurements, in fact the conductance values for the Au (I) compound determined in CH_2Cl_2, showed concentration-dependence in the range of 1.02–1.99 µS cm^{-1} (see Table 1), confirming the electrolytic nature of the complex.

The complexes **AuL2** and **AuL3** were prepared in the similar manner. In both cases in the FTIR spectra is observed the absorbance of –OH group around 3400 cm^{-1}, ^1H and ^{13}C NMR spectra show the expected signals (see attribution in the 'Experimental' section) with one sharp resonance for carbene of each complex at 178.9 and 185.0 ppm for **AuL2** and **AuL3**, respectively. The elemental analysis for two complexes (reported in 'Experimental' section) gives a ratio among ligand, gold and chloride of 1:1:1. MS spectra show the peak leading, associated each one with the respective 559 and 603 m/z for the complexes **AuL2** and **AuL3**, respectively. Conductivity measurements confirmed the electrolytic nature of the complexes. So it is likely also accepted as true that the structure of these complexes is similar to that of $([Ag(L1)_2]^+[AgCl_2]^-)$ [38,53].

AuL3 compound inhibits anchorage-dependent & anchorage-independent growth in MCF-7 breast cancer cells

We have initially examined the ability of the synthesized compounds to affect breast cancer cell

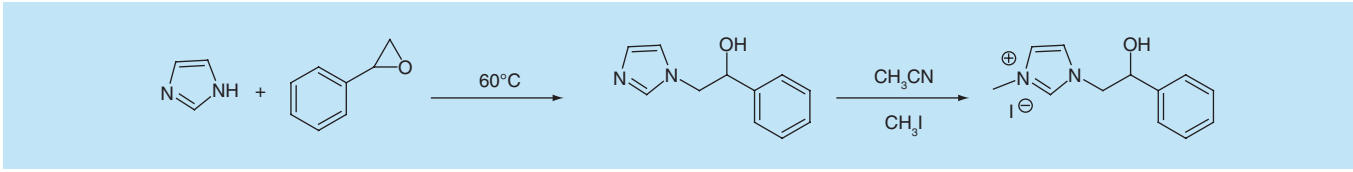

Figure 3. Synthesis of L3 salt: *N*-methyl-*N'*-[(2-hydroxy-2-phenyl)ethyl]-imidazole iodide.

proliferation. Since 70 to 80% of newly diagnosed breast cancers are ER and/or PR-positive, we used as experimental model the well-characterized ER/PR-positive MCF-7 breast cancer cell line. The effects of increasing concentrations of the different compounds (**AuL1**, **AgL1**, **AuL2**, **AgL2**, **AuL3** and **AgL3**) on MCF-7 cell proliferation were tested by using MTT assay. We observed that **AuL1** and **AgL1** as well as **AuL2** and **AgL2** treatments did not elicit any significant reduction in growth (Figure 5A & B). In contrast, **AuL3** and **AgL3** treatments for 72 h reduced MCF-7 cell viability in a dose-dependent manner (Figure 5C), with IC_{50} values equal to 1 and 4 μM, respectively (Table 2). In addition, the cytotoxicity of **AuL3** was compared with the one of the commonly used anticancer drugs *cis*-platin (data not shown). The results of continuous cisplatin exposure in MTT assays showed that it was able to produce 50% growth inhibition (IC_{50}) at 80.23 ± 5.3 μM in MCF-7 cells, indicating that **AuL3** was about 80-times more cytotoxic than *cis*-platin. A second approach we have employed was to evaluate the antiproliferative effects mediated by these compounds using anchorage-independent soft agar growth assay, an assay that better reflects *in vivo* 3D growth (Figure 5D). Consistently with the MTT assay data, **AuL3** and **AgL3** treatments significantly reduced colony formation in a dose-dependent manner, with the highest decrease induced by **AuL3**, whereas **AuL1**, **AgL1**, **AuL2** and **AgL2** treatments did not affect the capability of MCF-7 cells to form colonies in soft agar. Importantly, the prolonged **AuL3** and **AgL3** treatments up to 72 h induced no antiproliferative response in non tumorigenic MCF-10A breast epithelial cells (Figure 5E). Taken together, these results demonstrated that **AuL3** was the most active molecule in inducing growth inhibition in MCF-7 breast cancer cells, probably because of its lipophilic features and golden presence, compared with the other synthetized compounds.

AuL3 compound induces apoptosis in MCF-7 breast cancer cells

In order to determine the role of apoptosis in cell growth inhibition induced by **AuL3** treatment, we used two different approaches. First, we evaluated the proteolysis of PARP, a well-recognized cellular substrate of mammalian caspases, by immunoblotting analysis (Figure 6A). We found an increase in the levels of the proteolytic form of PARP (86 kDa) in MCF-7 breast cancer cells after **AuL3** treatment, as compared with the control. Second, the TUNEL assay was performed to assess DNA fragmentation as a key event in the process of apoptosis. As shown in Figure 6B, a high percentage of TUNEL-positive cells was observed in MCF-7 cells treated with **AuL3** at 1 μM of concentration. Mitochondria play a crucial role in the regulation of apoptosis and many chemotherapeutic agents that induce cell apoptosis trigger mitochondrial dysfunction when added to intact cells [56,57]. Interestingly, several gold-carbene complexes have been examined as anticancer agents with antimithocondrial activity [58]. Thus, we investigated whether the observed apoptotic effects induced by **AuL3** exposure in MCF-7 cells were due to impaired mitochondria. Mitochondria were labelled with a mitochondrial-targeted probe, MitoTracker Deep Red FM and mitochondrial staining was monitored. In nonapoptotic (vehicle-treated) cells, intact mitochondria exhibited a clear perinuclear red fluorescence; whereas in cells treated with **AuL3**, the fluorescence intensity of the probe decreased in a time-dependent manner, implying a reduction of mitochondrial content. Figure 6C shows the changes of MCF-7 cell fluorescence as a result of drug treatment. Consistently

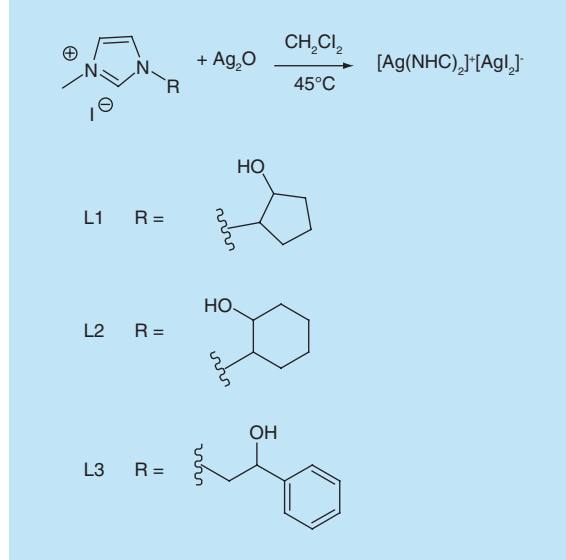

Figure 4. Synthetic scheme of Ag–NHC complexes (AgL1, Ag L2 and AgL3).

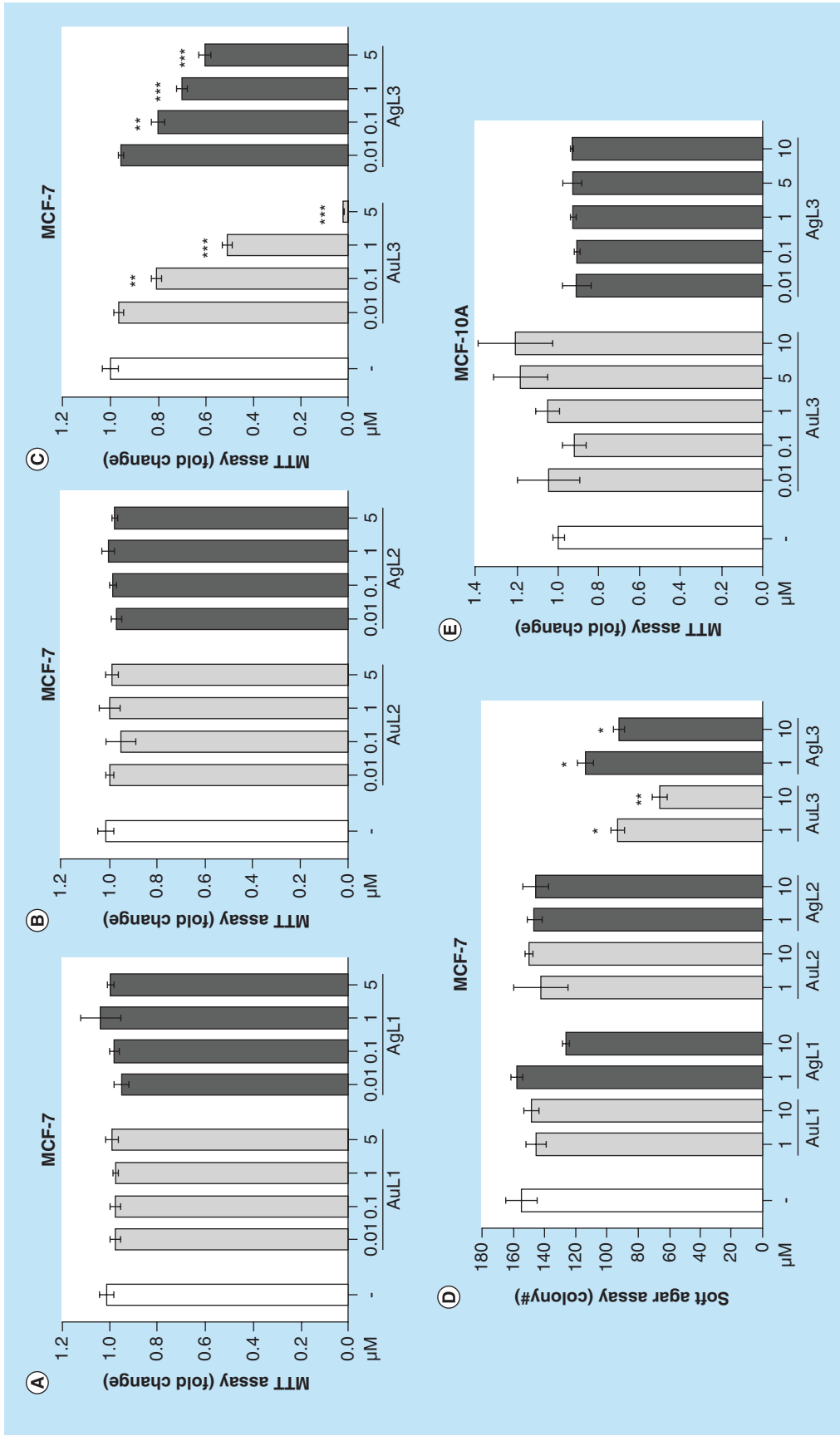

Figure 5. Effects of Au–NHC and Ag–NHC complexes on MCF-7 breast cancer cell growth. MTT assays in MCF-7 breast cancer cells treated with vehicle (-), or **AuL1/AgL1 (A)**, **AuL2/AgL2 (B)**, **AuL3/AgL3 (C)** at 0.01, 0.1, 1 and 5 μM of concentrations for 72 h. Cell proliferation is expressed as fold change compared with control (vehicle-treated cells). The values represent the means ± SD of three different experiments, each performed with triplicate samples. **(D)** MCF-7 cells were plated in soft agar and then treated with vehicle (-) or the different compounds as indicated. Cells were allowed to grow for 14 days and the number of colonies >50 μm were quantified and the results were graphed. Data are the mean colony number ± SD of three plates and representative of three independent experiments. **(E)** MTT assays in MCF-10A nontumorigenic breast epithelial cells treated with vehicle (-), or increasing concentrations of **AuL3** or **AgL3** (0.01, 0.1, 1, 5 and 10 μM) for 72 h. Cell proliferation is expressed as fold change compared with control (vehicle-treated cells). The values represent the means ± SD of three different experiments, each performed with triplicate samples.*p < 0.05; **p < 0.005; ***p < 0.0005. SD: Standard deviation.

Table 1. Values of conductance of $[(L1)_2Au]^+[AuCl_2]^-$ measured in CH_2Cl_2 at 25°C.

Concentration (mmol/l)	Conductivity (μS · cm^{-1})
3.31	1.02
4.41	1.58
5.43	1.91
6.55	1.66
8.18	1.52

with the release of cytochrome c into the extramitochondrial milieu under apoptotic conditions [59], a significant increase of cytochrome c levels in the cytosolic fractions of MCF-7 cells after 24 and 48 h of treatment with **AuL3** was detected (Figure 6D). The maintenance of mitochondrial integrity is highly dependent on the Bcl-2 family of proteins [60,61]. The expression levels of the antiapoptotic protein Bcl-2 were slightly decreased in **AuL3**-treated MCF-7 cells, whereas exposure of MCF-7 cells to AuL3 resulted in an increased expression of the proapoptotic proteins Bax and BID (Figure 6D). These results highlight the potential of **AuL3** compound to target the mitochondrial cell death pathway.

AuL3 treatment increases p53 & $p21^{WAF1/Cip1}$ expression in MCF-7 breast cancer cells

Since the tumor suppressor gene *p53* is required for checkpoint control during cell cycle progression in response to different factors and participates in the apoptotic cascade even by directly acting on multiple mitochondrial targets [62,63], we examined the potential ability of **AuL3** to modulate the expression of p53 along with its natural target gene $p21^{WAF1/Cip1}$. Cells were treated with **AuL3** at 0.1, 1 and 5 μM concentrations and whole cell lysates were then analyzed using immunoblotting analysis. As shown in Figure 7A, **AuL3** treatment significantly increased p53 and $p21^{WAF1/Cip1}$ protein expression. Accordingly, real-time RT-PCR revealed an induction of both *p53* and $p21^{WAF1/Cip1}$ mRNA levels in MCF-7 cells after 24-h treatment with all the different doses of **AuL3** (Figure 7B). These results prompted us to investigate whether the upregulatory effects of **AuL3** compound on p53 expression may be due to its ability to influence p53 gene transcriptional activity.

To evaluate whether **AuL3** may transactivate the *p53* promoter gene, MCF-7 cells were transiently transfected with a luciferase reporter construct (named as *p53*-1) containing the upstream region of the *p53* gene spanning from -1800 to +12 bp (Figure 8A) and treated with increasing concentrations of **AuL3** for 24 h. We observed a significant activation of *p53-1* after treatment with **AuL3** compound (Figure 8B). To identify the region within the *p53* promoter responsible for **AuL3**-mediated transactivation, we performed functional assays using *p53*-deleted constructs containing putative binding motifs for CTF-1/YY1, NF-Y, NFκB and Sp1-like proteins (GC) (schematically shown in Figure 8A). The responsiveness to **AuL3** compound was still maintained in cells transfected with the *p53*–6 plasmid encoding the region from -106 to +12, whereas it was no longer observed in the presence of the *p53*–13 construct encoding the sequence from -106 to -40 (Figure 8C). Therefore, the region from -40 to +12, which contains the GC-rich/Sp1 motifs, was required for mediating the stimulatory effects of **AuL3** on *p53* promoter gene expression. To confirm the specific involvement of Spl region in AuL3-mediated *p53* transactivation, ChIP assays were performed. Using specific antibodies against Spl, and RNA-polymerase II, protein–chromatin complexes were immunoprecipitated from cells treated with or without **AuL3** compound for 3 h. The resulting precipitated DNA was then quantified using real-time PCR with primers spanning the Spl-binding element within the *p53* promoter region. As shown in Figure 8D, Spl recruitment was significantly increased upon **AuL3** treatment. These results were well correlated with an enhanced association of RNA-polymerase II to the *p53* regulatory region (Figure 8E). Our findings demonstrated that the ability of **AuL3** compound to stimulate *p53* transcription is dependent on the transcription factor Spl.

Table 2. IC_{50} of AuL3 and AgL3 compounds for MCF-7 and ZR-75–1 breast cancer cells on anchorage-dependent growth.

Cell lines	IC_{50} (μmol/l) AuL3	95% CI	IC_{50} (μmol/l) AgL3	95% CI
MCF-7	1	0.8–1.2	4	2.1–5.8
ZR-75–1	2.6	2.2–3.2	–	–

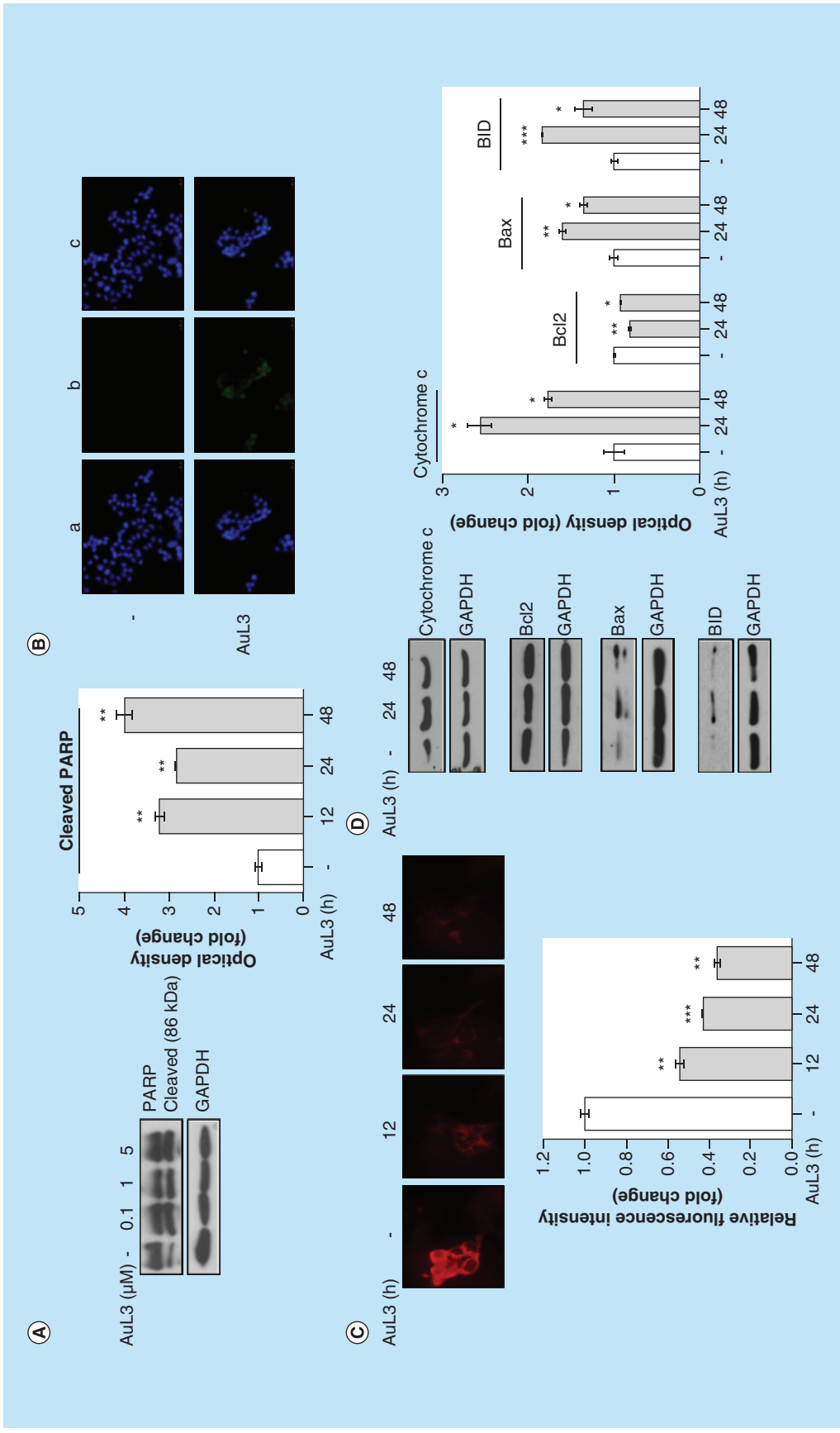

Figure 6. Apoptotic effects of AuL3 compound in MCF-7 breast cancer cells. (A) Left panel, immunoblot of PARP protein from extracts of MCF-7 cells treated with vehicle (-) or **AuL3** at 0.1, 1 and 5 μM of concentrations for 24 h. GAPDH was used as control for equal loading and transfer. Right panel, the histograms represent the means ± SD of three separate experiments in which band intensities were evaluated in terms of optical density arbitrary units and expressed as fold change compared with vehicle-treated samples and normalized for GAPDH content. **(B)** MCF-7 cells were treated with vehicle (-) or **AuL3** at a concentration of 1 μM for 24 h. After treatment, cells were cold-methanol fixed and subjected to TUNEL assay. After DAPI incubation to stain nuclei, fixed cell were observed and imaged under an inverted fluorescence microscope (20× magnification): a) TUNEL staining, b) DAPI, c) overlay. Images are representative of three separate experiments. **(C)** Mitochondria staining with MitoTracker Deep Red Fluorescent probe in cells treated with vehicle (-) or **AuL3** at 1 μM for 12, 24 and 48 h. Fluorescence images are shown (upper panel) and fluorescence levels are quantitated (lower panel) from three separate experiments. **(D)** Left panel, immunoblot of cytochrome c, Bcl2, Bax and BID from extracts of MCF-7 cells treated with vehicle (-) or **AuL3** at 1 μM for 24 and 48 h. GAPDH was used as control for equal loading and transfer. Right panel, the histograms represent the means ± SD of three separate experiments in which band intensities were evaluated in terms of optical density arbitrary units and expressed as fold change compared with vehicle-treated samples and normalized for GAPDH content. *$p < 0.05$; **$p < 0.005$; ***$p < 0.0005$.

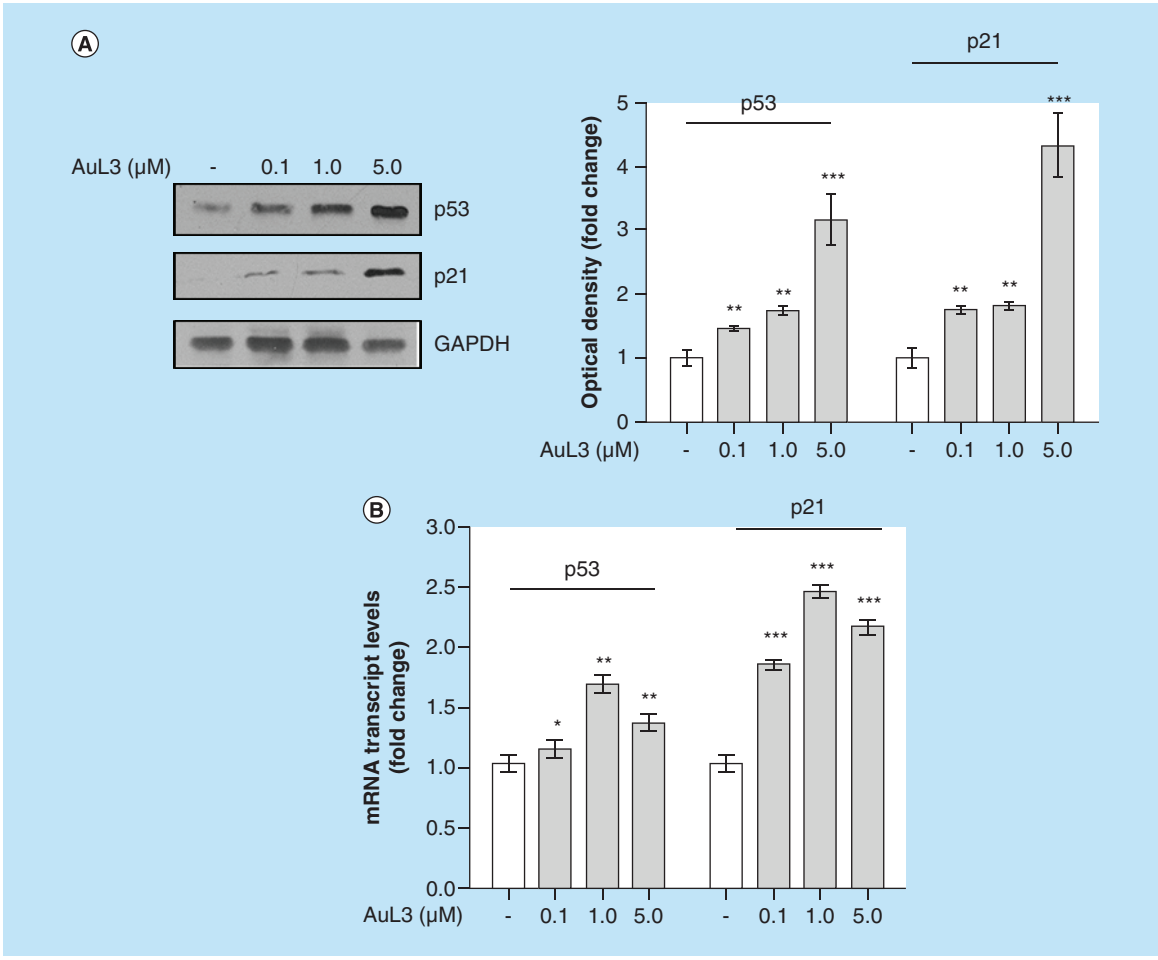

Figure 7. Upregulation of p53 and p21 expression by AuL3 compound in MCF-7 breast cancer cells. (A) Left panel, immunoblots of p53 and p21$^{WAF1/Cip1}$ from extracts of MCF-7 cells treated with vehicle (-) or **AuL3** at 0.1, 1 and 5 μM of concentrations for 48 h. GAPDH was used as a control for equal loading and transfer. Right panel, the histograms represent the mean ± SD of three separate experiments in which band intensities were evaluated in terms of optical density arbitrary units and expressed as fold change compared with vehicle-treated samples and normalized for GAPDH content. **(B)** *p53* and *p21* $^{WAF1/Cip1}$ mRNA expression, evaluated by real-time RT-PCR, in MCF-7 cells treated with vehicle (-) or **AuL3** (0.1, 1, 5 μM) for 24 h. Each sample was normalized to its *GAPDH* mRNA content. *p < 0.05; **p < 0.005: ***p < 0.0005.

Sp1 is a well-investigated factor that has been shown to be involved through the transcriptional regulation of many genes in several cellular processes, including cell differentiation, growth and apoptosis [64]. Because of the Sp1-dependent upregulatory effects on *p53* gene transcription mediated by **AuL3** compound, we evaluated the potential binding mode of **AuL3** to Spl by molecular docking studies using as molecular target, the Zinc finger domain of Sp1 (PDB code 1SP1) [65]. We also evaluated docking interaction of **AgL3** with Sp-1. The binding site center was positioned as the OG atom of Ser 19 and the volume encompassed by 20Å from that atom was considered as the binding cleft. **AuL3** and **AgL3** have a similar binding mode to Sp1 (Figure 9A & B). The top ranked poses show a fitness ranking of 61.34 and 57.93, respectively. Both the **AuL3** and **AgL3** moieties form hydrogen bond with Ser 19 residue and halogen bond with Lys 23 residue, hydrophobic interactions with Ile 22 and a π–π stacking with Phe 3 (Figure 9A & B). A small displacement of the silver atom with respect to the gold atom was the only significant difference between the two poses (Figure 9C), this would affect the lesser antitumor activity of **AgL3** respect to **AuL3**.

Effects of AuL3 in ZR-75–1 breast cancer cells

To extend the results obtained, we tested the effects of **AuL3** compound in affecting growth of another human ERα-positive breast cancer cell line, named as ZR-75–1 cells. By using MTT assay, we demonstrated that **AuL3** compound for 72 h inhibited cell survival

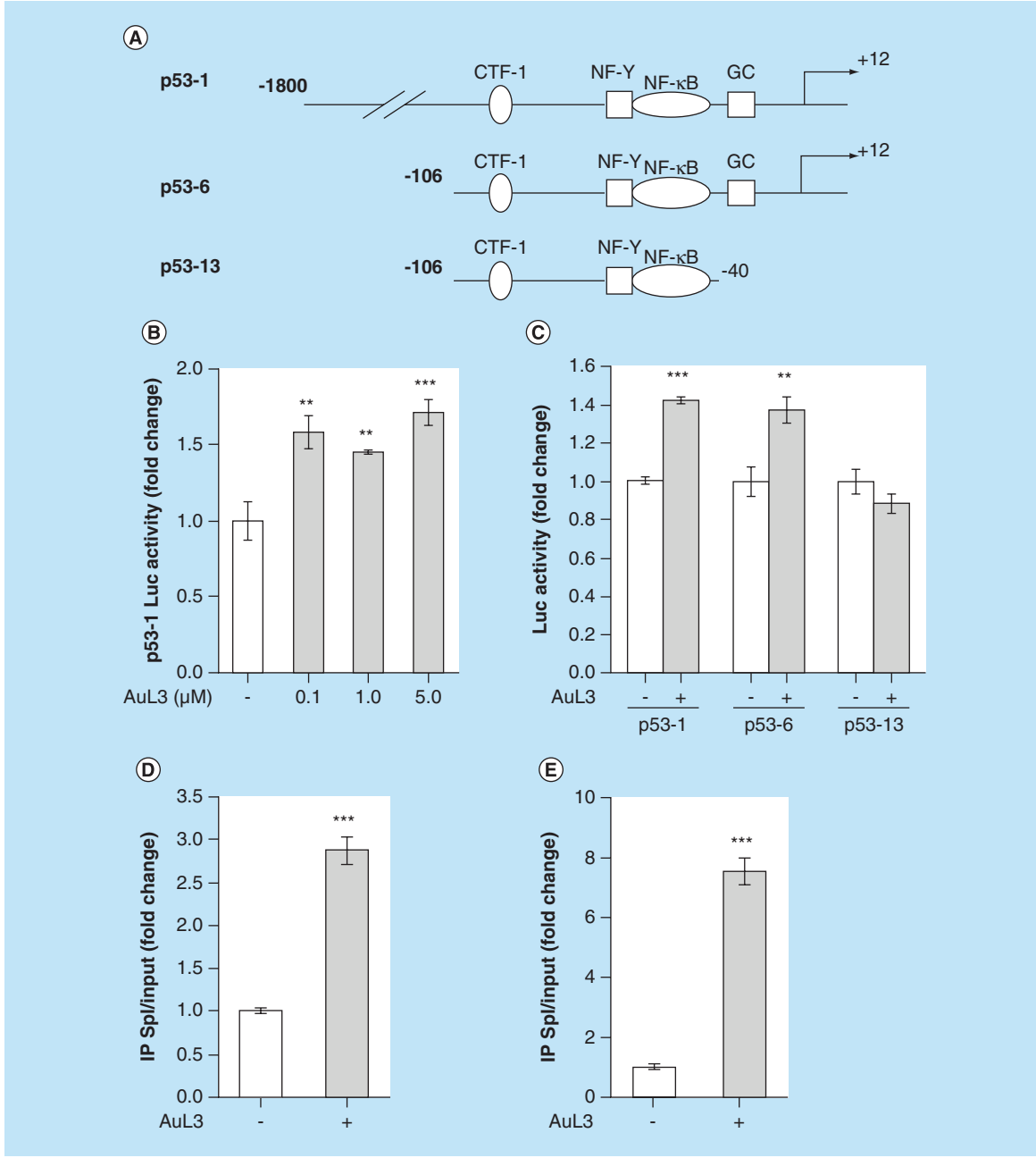

Figure 8. Effects of AuL3 compound on *p53* gene promoter luciferase reporter constructs. (A) Schematic map of the *p53* promoter fragments used in this study. **(B)** MCF-7 cells were transiently transfected with *p53* gene promoter luciferase reporter construct *p53*-1 and treated for 24 h with vehicle (-) or **AuL3** at 0.1, 1 and 5 μM of concentrations. **(C)** MCF-7 cells were transiently transfected with *p53* gene promoter luciferase reporter constructs (*p53*-1, *p53*-6, *p53*-13) and treated for 24 h with vehicle (-) or **AuL3** (1 μM). The luciferase activities were normalized to the *Renilla* luciferase as internal transfection control and data were reported as fold change. MCF-7 cells were treated with vehicle (-) or **AuL3** (1 μM, 3 h), then crosslinked with formaldehyde and lysed. The precleared chromatin was immunoprecipitated with anti-Spl **(D)**, and anti-RNA polymerase II **(E)** antibodies. A 5 μl volume of each sample and input was analyzed by real-time PCR using specific primers to amplify *p53* promoter sequence, including the GC-rich motif. Columns are the means ± SD of three independent experiments, each performed in triplicate. **p < 0.005; ***p < 0.0005.
CTF-1: CCAAT-binding transcription factor-1; GC: GC-rich motif; NFκB: Nuclear factor-κB; NF-Y: Nuclear factor-Y.

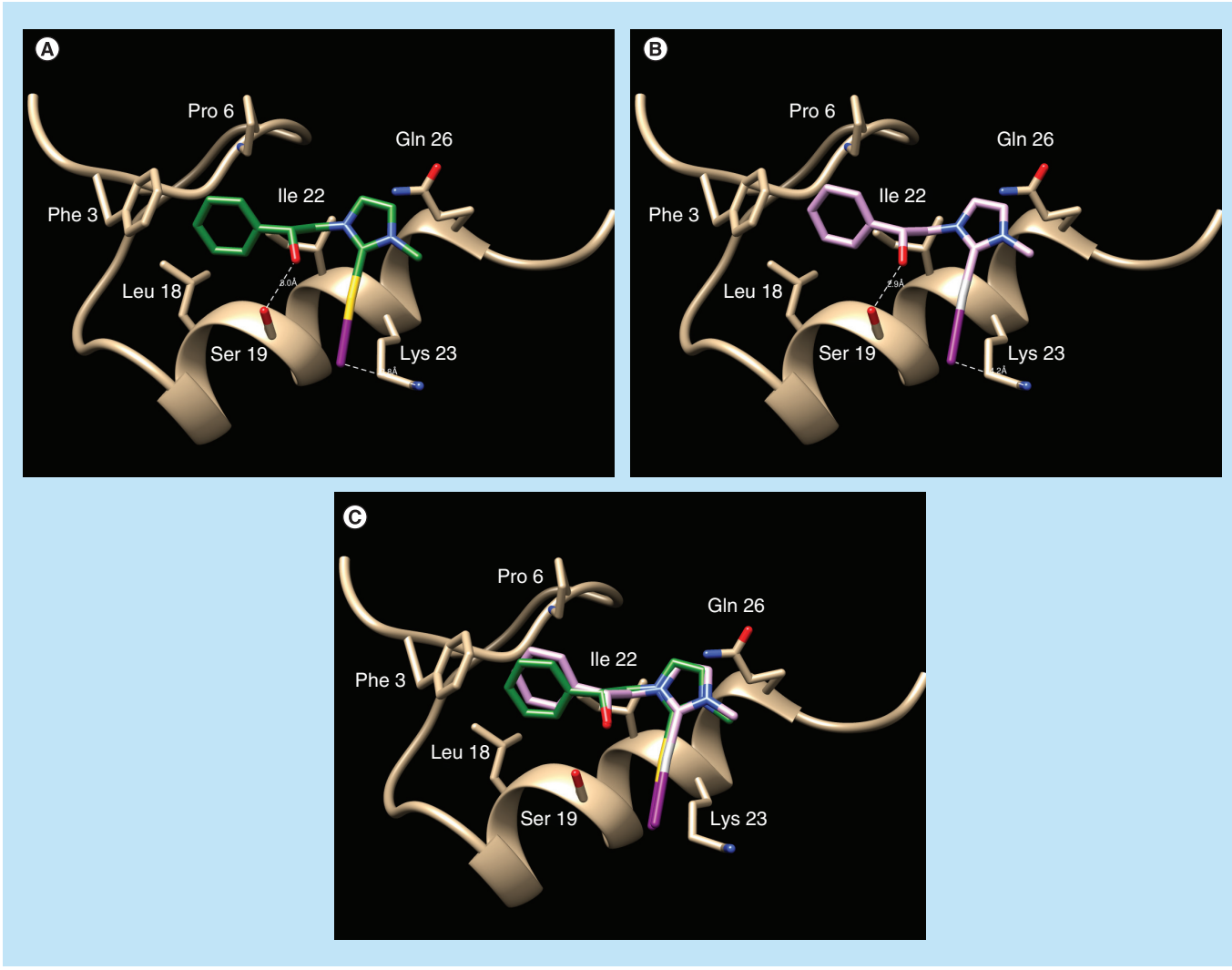

Figure 9. Binding mode of AuL3 and AgL3 to Sp1 zinc finger domain. The 3D structure of the Zinc finger domain from Transcription Factor Sp1 is reported as a brown ribbon. Residues involved in ligand binding are evidenced as sticks. **(A)** and **(B)** report the poses of **AuL3** and **AgL3**, respectively. The two binding modes are superposed in **(C)**.

in a dose-dependent fashion with IC_{50} values equal to 2.6 μM (Figure 10A & Table 2). In addition, as previously shown for MCF-7 cells, we found augmented PARP cleaved levels as well as increased expression of both p53 and $p21^{WAF1/Cip1}$ proteins in ZR-75-1 cells after treatment with increasing concentrations of **AuL3** (Figure 10B). These data confirmed that **AuL3** compound inhibits cell growth and induces apoptosis in different breast cancer cell background through p53 upregulation.

Conclusion

Herein, we have reported the synthesis and the biological evaluation of three silver NHC and of three new gold NHC complexes as valid therapeutic tools against breast cancer progression. These metallopharmaceuticals were projected introducing lipophilic substituents on the carbene structure in order to increase the ability to cross the biological membranes. As demonstrated, the most active antitumor compounds were **AgL3** and **AuL3**, holding a lipophilic structure, and they did not affect the proliferation of nontumorigenic epithelial breast cells. Particularly, **AuL3** exhibited lower IC_{50} values (1 and 2.6 μM, on MCF-7 and ZR-75-1 breast cancer cells, respectively) respect to **AgL3**, suggesting the importance of gold for the higher antitumor activity. Moreover, we have demonstrated that the antitumor activity of **AuL3** is due to the upregulation of p53 and $p21^{WAF1/Cip1}$ expression, dependent on the transcription factor Spl. The role of Sp1 has been further confirmed by molecular docking studies. These outcomes are interesting in the metallopharmaceutics research and open up a wide range of possibilities

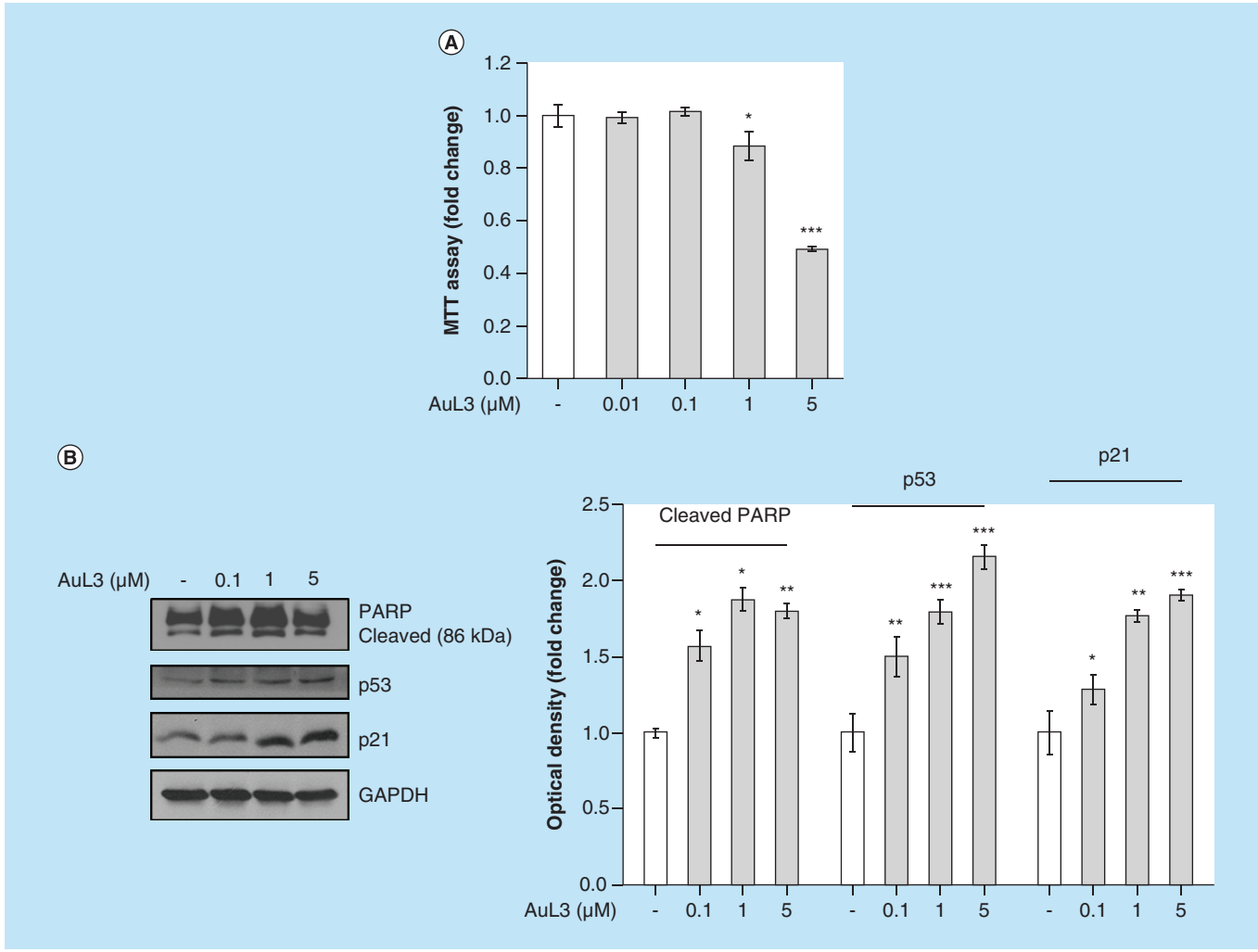

Figure 10. Effects of AuL3 treatment on ZR-75-1 breast cancer cell growth. (A) MTT assays in ZR-75-1 breast cancer cells treated with vehicle (-), or increasing concentrations of **AuL3** (0.01, 0.1, 1 and 5 μM) for 72 h. Cell proliferation is expressed as fold change compared with control (vehicle-treated cells). The values represent the means ± SD of three different experiments, each performed with triplicate samples. **(B)** Left panel, immunoblots showing PARP, p53 and p21$^{WAF1/CiP1}$ protein expression from extracts of ZR-75-1 cells treated with vehicle (-) or **AuL3** at 0.1, 1 and 5 μM of concentrations for 48 h. GAPDH was used as a control for equal loading and transfer. Right panel, the histograms represent the mean ± SD of three separate experiments in which band intensities were evaluated in terms of optical density arbitrary units and expressed as fold change compared with vehicle-treated samples and normalized for GAPDH content. *$p < 0.05$; **$p < 0.005$; ***$p < 0.0005$.

to obtain versatile carbene complexes, with a variety of ligands that may provide a novel arsenal of useful anticancer tools as a valid alternative to the most used *cis*-platin.

Future perspective

These outcomes may be enlarged in order to ameliorate the antitumor activity and diminish the toxicity of metal complex-based drugs. In this way, new classes of anticancer compounds able to act on specific targets will be developed and used as valid therapeutic strategies to the most traditional chemotherapeutic agents.

Financial & competing interests disclosure

This work was supported by ex 60% MIUR (MS Sinicropi), Fondazione Italiana per la Ricerca sul Cancro (AIRC) grants: IG #11595 (S Andò), MFAG #16899 (I Barone), FARB2015 (C Saturnino). The authors have no relevant affiliations or financial involvement with any organization or entity with a financial interest in or financial conflict with the subject matter or materials discussed in the manuscript. This includes employment, consultancies, honoraria, stock ownership or options, expert testimony, grants or patents received or pending, or royalties.

No writing assistance was utilized in the production of this manuscript.

Executive summary

- Three silver and three new gold *N*-heterocyclic carbene complexes were reported.
- The three new gold *N*-heterocyclic carbene complexes were synthesized by transmetallation reaction.
- **AuL3** inhibits breast cancer growth and triggers apoptosis.
- Mechanistically, **AuL3** induces Sp1-mediated *p53* upregulation.

References

Papers of special note have been highlighted as:
• of interest; •• of considerable interest

1 Ferlay J, Soerjomataram I, Dikshit R *et al.* Cancer incidence and mortality worldwide: sources, methods and major patterns in GLOBOCAN 2012. *Int. J. Cancer.* 136(5), E359–E386 (2015).

2 Berners-Price SJ. Activating platinum anticancer complexes with visible light. *Angew. Chem. Int. Edit. Engl.* 50(4), 804–805 (2011).

3 Sirignano E, Saturnino C, Botta A *et al.* Synthesis, characterization and cytotoxic activity on breast cancer cells of new half-titanocene derivatives. *Bioorg. Med. Chem. Lett.* 23(11), 3458–3462 (2013).

4 Napoli M, Saturnino C, Sirignano E, Popolo A, Pinto A, Longo P. Synthesis, characterization and cytotoxicity studies of methoxy alkyl substituted metallocenes. *Eur. J. Med. Chem.* 46(1), 122–128 (2011).

5 Saturnino C, Napoli M, Paolucci G *et al.* Synthesis and cytotoxic activities of group 3 metal complexes having monoanionic tridentate ligands. *Eur. J. Med. Chem.* 45(9), 4169–4174 (2010).

6 Grisi F, Costabile C, Grimaldi A, Viscardi C, Saturnino C, Longo P. Synthesis of unsaturated macrocycles by Ru-catalyzed ring-closing metathesis: a comparative study. *Eur. J. Org. Chem.* 30, 5928–5934 (2012).

7 Saturnino C, Sirignano E, Botta A *et al.* New titanocene derivatives with high antiproliferative activity against breast cancer cells. *Bioorg. Med. Chem. Lett.* 24(1), 136–140 (2014).

8 Chimento A, Saturnino C, Iacopetta D *et al.* Inhibition of human topoisomerase I and II and anti-proliferative effects on MCF-7 cells by new titanocene complexes. *Bioorg. Med. Chem.* 23(22), 7302–7312 (2015).

9 Sirignano E, Pisano A, Caruso A *et al.* Different 6-aryl-fulvenes exert anti-proliferative effects on cancer cells. *Anti-cancer Agents Med.* 15(4), 468–474 (2015).

10 Hu CQ, Li X, Wang W, Zhang RY, Deng LP. Metal-N-heterocyclic carbene complexes as anti-tumor agents. *Curr. Med. Chem.* 21(10), 1220–1230 (2014).

11 Gautier A, Cisnetti F. Advances in metal-carbene complexes as potent anti-cancer agents. *Metallomics* 4(1), 23–32 (2012).

12 Perfetto A, Costabile C, Longo P, Bertolasi V, Grisi F. Probing the relevance of NHC ligand conformations in the Ru-catalysed ring-closing metathesis reaction. *Chem. Eur. J.* 19(32), 10492–10496 (2013).

• **Reports the preparation of suitable substituted N-heterocyclic carbene (NHC) backbone.**

13 Fischer EO. On the way of carbene and carbyne complexes. *Adv. Organomet. Chem.* 14, 1–32 (1976).

14 Guggenberger LJ, Schrock RR. Structure of bis(cyclopentadienyl)methylmethylenetantalum and the estimated barrier to rotation about the tantalum–methylene bond. *J. Am. Chem. Soc.* 97(22), 6578–6579 (1975).

15 Schrock RR, Fellmann JD. Multiple metal-carbon bonds. 8. Preparation, characterization, and mechanism of formation of the tantalum and niobium neopentylidene complexes, M(CH2CMe3)3(CHCMe3). *J. Am. Chem. Soc.* 100(11), 3359–3370 (1978).

16 Arduengo AJ Ill, Harlow RL, Kline M. A stable crystalline carbene. *J. Am. Chem. Soc.* 113, 361–363 (1991).

17 Cavallo L, Correa A, Costabile C, Jacobsen H. Steric and electronic effects in the bonding of N-heterocyclic ligands to transition metals. *J. Organomet. Chem.* 690(24), 5407–5413 (2005).

18 Hu XL, Castro-Rodriguez I, Olsen K, Meyer K. Group 11 metal complexes of N-heterocyclic carbene ligands: nature of the metal-carbene bond. *Organometallics* 23(4), 755–764 (2004).

19 Nemcsok D, Wichmann K, Frenking G. The significance of pi interactions in group 11 complexes with N-heterocyclic carbenes. *Organometallics* 23(15), 3640–3646 (2004).

20 Oehninger L, Rubbiani R, Ott I. N-heterocyclic carbene metal complexes in medicinal chemistry. *Dalton Trans.* 42(10), 3269–3284 (2013).

21 Patil SA, Patil SA, Patil R *et al.* N-heterocyclic carbene metal complexes as bio-organometallic antimicrobial and anticancer drugs. *Future Med. Chem.* 7(10), 1305–1333 (2015).

•• **Focuses on the current development and advances in the preparation/characterization of NHC–metal complexes and their biomedical potential.**

22 Parisi OI, Morelli C, Puoci F *et al.* Magnetic molecularly imprinted polymers (MMIPs) for carbazole derivative release in targeted cancer therapy. *J. Mater. Chem. B* 2(38), 6619–6625 (2014).

23 Bruno G, Nicolo F, Loschiavo S, Sinicropi MS, Tresoldi G. Synthesis and spectroscopic properties of Di-2-Pyridyl Sulfide (Dps) compounds - crystal-structure of [Ru(Dps)2cl2]. *J. Chem. Soc. Dalton Trans. Rans.* 1, 17–24 (1995).

24 Klasen HJ. A historical review of the use of silver in the treatment of burns. II. Renewed interest for silver. *Burns* 26(2), 131–138 (2000).

25 Melaiye A, Simons RS, Milsted A *et al.* Formation of water-soluble pincer silver(I)-carbene complexes: a novel antimicrobial agent. *J. Med. Chem.* 47(4), 973–977 (2004).

26 Hindi KM, Siciliano TJ, Durmus S *et al.* Synthesis, stability, and antimicrobial studies of electronically tuned silver acetate N-heterocyclic carbenes. *J. Med. Chem.* 51(6), 1577–1583 (2008).

27 Youngs WJ, Knapp AR, Wagers PO, Tessier CA. Nanoparticle encapsulated silver carbene complexes and their antimicrobial and anticancer properties: a perspective. *Dalton Trans.* 41(2), 327–336 (2012).

28 Medvetz DA, Hindi KM, Panzner MJ, Ditto AJ, Yun YH, Youngs WJ. Anticancer Activity of Ag(I) N-heterocyclic carbene complexes derived from 4,5-dichloro-1h-imidazole. *Met. Based Drugs* 2008, 384010 (2008).

29 Li Y, Liu GF, Tan CP, Ji LN, Mao ZW. Antitumor properties and mechanisms of mitochondria-targeted Ag(I) and Au(I) complexes containing N-heterocyclic carbenes derived from cyclophanes. *Metallomics* 6(8), 1460–1468 (2014).

30 Talib J, Beck JL, Ralph SF. A mass spectrometric investigation of the binding of gold antiarthritic agents and the metabolite [Au(CN)2]- to human serum albumin. *J. Biol. Inorg. Chem.* 11(5), 559–570 (2006).

31 Ozdemir I, Denizci A, Ozturk HT, Cetinkaya B. Synthetic and antimicrobial studies on new gold(I) complexes of imidazolidin-2-ylidenes. *Appl. Organomet. Chem.* 18(7), 318–322 (2004).

32 Yan JJ, Chow ALF, Leung CH, Sun RWY, Ma DL, Che CM. Cyclometalated gold(III) complexes with N-heterocyclic carbene ligands as topoisomerase I poisons. *Chem. Commun.* 46(22), 3893–3895 (2010).

33 Wang CH, Shih WC, Chang HC *et al.* Preparation and characterization of amino-linked heterocyclic carbene palladium, gold, and silver complexes and their use as anticancer agents that act by triggering apoptotic cell death. *J. Med. Chem.* 54(14), 5245–5249 (2011).

34 Das Adhikary S, Bose D, Mitra P, Das Saha K, Bertolasi V, Dinda J. Au(I)- and Pt(II)-N-heterocyclic carbene complexes with picoline functionalized benzimidazolin-2-ylidene ligands; synthesis, structures, electrochemistry and cytotoxicity studies. *New J. Chem.* 36(3), 759–767 (2012).

35 Mui YF, Fernandez-Gallardo J, Elie BT *et al.* Titanocene-gold complexes containing n-heterocyclic carbene ligands inhibit growth of prostate, renal, and colon cancers *in vitro*. *Organometallics* 35(9), 1218–1227 (2016).

36 Nandy A, Dey SK, Das S, Munda RN, Dinda J, Das Saha K. Gold (I) N-heterocyclic carbene complex inhibits mouse melanoma growth by p53 upregulation. *Mol. Cancer* 13, 57 (2014).

- **Shows the '*in vitro*' and '*in vivo*' antimelanoma properties of a newly synthesized Au–NHC complex.**

37 Hahn FE, Jahnke MC. Heterocyclic carbenes: synthesis and coordination chemistry. *Angew. Chem. Int. Edit. Engl.* 47(17), 3122–3172 (2008).

38 Napoli M, Saturnino C, Cianciulli EI *et al.* Silver(I) N-heterocyclic carbene complexes: synthesis, characterization and antibacterial activity. *J. Organomet. Chem.* 725, 46–53 (2013).

- **Reports the synthesis of new silver complexes with stability to hydrolysis and antibacterial activity.**

39 Baker MV, Barnard PJ, Berners-Price SJ *et al.* Synthesis and structural characterisation of linear Au(I) N-heterocyclic carbene complexes: new analogues of the Au(I) phosphine drug Auranofin. *J. Organomet. Chem.* 690(24–25), 5625–5635 (2005).

40 Schuttelkopf AW, van Aalten DM. PRODRG: a tool for high-throughput crystallography of protein-ligand complexes. *Acta Crystallogr. D Biol. Crystallogr.* 60(Pt 8), 1355–1363 (2004).

41 Sinicropi MS, Lappano R, Caruso A *et al.* (6-bromo-1,4-dimethyl-9H-carbazol-3-yl-methylene)-hydrazine (carbhydraz) acts as a GPER agonist in breast cancer cells. *Curr. Top. Med. Chem.* 15(11), 1035–1042 (2015).

42 Pettersen EF, Goddard TD, Huang CC *et al.* UCSF Chimera – a visualization system for exploratory research and analysis. *J. Comput. Chem.* 25(13), 1605–1612 (2004).

43 Iacopetta D, Madeo M, Tasco G *et al.* A novel subfamily of mitochondrial dicarboxylate carriers from *Drosophila melanogaster*: biochemical and computational studies. *Biochim. Biophys. Acta* 1807(3), 251–261 (2011).

44 Qin CH, Nguyen T, Stewart J, Samudio I, Burghardt R, Safe S. Estrogen up-regulation of p53 gene expression in MCF-7 breast cancer cells is mediated, by calmodulin kinase IV-dependent activation of a nuclear factor kappa B/CCAAT-binding transcription factor-1 complex. *Mol. Endocrinol.* 16(8), 1793–1809 (2002).

45 Sala M, Chimento A, Saturnino C *et al.* Synthesis and cytotoxic activity evaluation of 2,3-thiazolidin-4-one derivatives on human breast cancer cell lines. *Bioorg. Med. Chem. Lett.* 23(17), 4990–4995 (2013).

46 Sinicropi MS, Caruso A, Conforti F *et al.* Synthesis, inhibition of NO production and antiproliferative activities of some indole derivatives. *J. Enz. Inhib. Med. Ch.* 24(5), 1148–1153 (2009).

47 Caruso A, Chimento A, El-Kashef H *et al.* Antiproliferative activity of some 1,4-dimethylcarbazoles on cells that express estrogen receptors: part I. *J. Enz. Inhib. Med. Ch.* 27(4), 609–613 (2012).

48 Grande F, Barone I, Aiello F *et al.* Identification of novel 2-(1H-indol-1-yl)-benzohydrazides CXCR4 ligands impairing breast cancer growth and motility. *Fut. Med. Chem.* 8(2), 93–106 (2016).

- **Highlights the identification and synthesis of leads useful for a rational design of broad-spectrum therapeutics active in breast cancer.**

49 Rechoum Y, Rovito D, Iacopetta D *et al.* AR collaborates with ERalpha in aromatase inhibitor-resistant breast cancer. *Breast Cancer Res. Tr.* 147(3), 473–485 (2014).

50 Gu GW, Barone I, Gelsomino L *et al. Oldenlandia diffusa* extracts exert antiproliferative and apoptotic effects on human breast cancer cells through ER alpha/Sp1-mediated p53 activation. *J. Cell. Physiol.* 227(10), 3363–3372 (2012).

51 Arnold PL, Rodden M, Davis KM, Scarisbrick AC, Blake AJ, Wilson C. Asymmetric lithium(I) and copper(II) alkoxy-N-heterocyclic carbene complexes; crystallographic characterisation and Lewis acid catalysis. *Chem. Commun.* (14), 1612–1613 (2004).

52 Bocchino C, Napoli M, Costabile C, Longo P. Synthesis of octahedral zirconium complex bearing [NHC-O]

ligands, and its behavior as catalyst in the polymerization of olefins. *J. Polym. Sci. Pol. Chem.* 49(4), 862–870 (2011).

53 Mariconda A, Grisi F, Costabile C, Falcone S, Bertolasi V, Longo P. Synthesis, characterization and catalytic behaviour of a palladium complex bearing a hydroxy-functionalized N-heterocyclic carbene ligand. *New J. Chem.* 38(2), 762–769 (2014).

•• **Shows the synthetic route to obtain complexes possessing functionalized, unsymmetrical substituted NHC ligand and transmetallation reaction.**

54 Kascatan-Nebioglu A, Panzner MJ, Tessier CA, Cannon CL, Youngs WJ. N-Heterocyclic carbene-silver complexes: a new class of antibiotics. *Coordin. Chem. Rev.* 251(5), 884–895 (2007).

55 Wang HMJ, Lin IJB. Facile synthesis of silver(I)-carbene complexes. Useful carbene transfer agents. *Organometallics* 17(5), 972–975 (1998).

56 Makin G, Dive C. Recent advances in understanding apoptosis: new therapeutic opportunities in cancer chemotherapy. *Trends Mol. Med.* 9(6), 251–255 (2003).

57 Debatin KM, Poncet D, Kroemer G. Chemotherapy: targeting the mitochondrial cell death pathway. *Oncogene* 21(57), 8786–8803 (2002).

58 Barnard PJ, Baker MV, Berners-Price SJ, Day DA. Mitochondrial permeability transition induced by dinuclear gold(I)-carbene complexes: potential new antimitochondrial antitumour agents. *J. Inorg. Biochem.* 98(10), 1642–1647 (2004).

59 Gogvadze V, Orrenius S, Zhivotovsky B. Multiple pathways of cytochrome c release from mitochondria in apoptosis. *Biochim. Biophys. Acta* 1757(5), 639–647 (2006).

60 Brenner D, Mak TW. Mitochondrial cell death effectors. *Curr. Opin. Cell Biol.* 21(6), 871–877 (2009).

61 Czabotar PE, Lessene G, Strasser A, Adams JM. Control of apoptosis by the BCL-2 protein family: implications for physiology and therapy. *Nat. Rev. Mol. Cell. Biol.* 15(1), 49–63 (2014).

62 Mihara M, Erster S, Zaika A *et al.* p53 has a direct apoptogenic role at the mitochondria. *Mol. Cell* 11(3), 577–590 (2003).

63 Murphy ME, Leu JIJ, George DL. p53 moves to mitochondria – a turn on the path to apoptosis. *Cell Cycle* 3(7), 836–839 (2004).

64 Suske G. The Sp-family of transcription factors. *Gene* 238(2), 291–300 (1999).

65 Narayan VA, Kriwacki RW, Caradonna JP. Structures of zinc finger domains from transcription factor Sp1 – insights into sequence-specific protein-DNA recognition. *J. Biol. Chem.* 272(12), 7801–7809 (1997).